Journal of Hydrology 634 (2024) 131111

Contents lists available at ScienceDirect

Journal of Hydrology

journal homepage: www.elsevier.com/locate/jhydrol

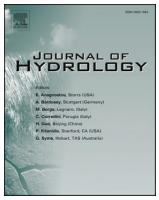

Reactive contaminant infiltration under dynamic preferential flow

Darrell W.S. Tang [a,*], Helen K. French [b], Anton Leijnse [a], Ruud P. Bartholomeus [a,c], Sjoerd E.A.T. M. van der Zee [a]

[a] Soil Physics and Land Management, Wageningen University, Wageningen, the Netherlands
[b] Faculty of Environmental Sciences and Natural Resource Management, Norwegian University of Life Sciences, Ås, Norway
[c] KWR Water Research Institute, Nieuwegein, the Netherlands

ARTICLE INFO

Keywords:
Soil contamination
Multicomponent biodegradation
Transient flow
Heterogeneous soil
Preferential flow
Contaminant leaching

ABSTRACT

Biodegradation is an important mechanism of contaminant removal from soils. We use numerical simulations to study the contaminant transport in heterogeneous soils subject to transient flow conditions and anaerobic multicomponent biodegradation. These processes and their interactions affect contaminant travel times, the extent of reactant mixing, solute and microbial biomass distributions in the soil, and biodegradation outcomes. Especially when flux variations are large, the combination of soil heterogeneity and transient flow gives rise to dynamic preferential flow zones, which affects reactant mixing and biodegradation outcomes. Results show that soil heterogeneity may reduce contaminant leaching due to enhanced reactant mixing, especially when biodegradation is more limited by reactant mixing. Furthermore, unlike under steady-state flow, under transient flow soil heterogeneity does not substantially reduce contaminant residence times. As preferential flow zones change dynamically, the spatio-temporally averaged transport, mixing, and biodegradation experienced by various parts of contaminant plumes become homogenized. Therefore, knowing the initial biodegradation rate of a contaminant upon infiltration, and its mean residence time in the soil, enables a relative sensitivity analysis. This allows biodegradation outcomes of various scenarios to be approximately ranked, even under soil heterogeneity and transient flow, using information that is straightforward to measure or estimate in the field.

1. Introduction

Contaminants that enter the soil may eventually leach to groundwater (Kass et al., 2005; Tang et al., 2023) if not biodegraded on the way down. Microbes in soils may biodegrade organic contaminants by oxidising them, a process which requires the presence of aqueous electron acceptors such as oxygen (Mulligan & Yong, 2004; Singh, 2008), nitrate (Shen et al., 2015), sulphate (Widdel et al., 2007), manganese (Schotanus et al., 2014), and ferric iron (Ramalingam & Cupples, 2020). However, soils are not well-mixed (Li et al., 2006; Acharya et al., 2005). Hence, even when all the necessary components for multicomponent biodegradation (contaminant, electron acceptor, microbes) are present in the soil, their spatial distributions might not overlap, and biodegradation may not occur. Furthermore, the rate of the biodegradation reaction depends on the concentration of all participating reactants (e.g. Blum et al., 2009). Hence, for such biodegradation processes to contribute significantly towards soil remediation, it is necessary for the plumes of contaminants, microbes, and electron acceptors to spatially overlap to a sufficient extent. In other words, these reactants must mix in order for the biodegradation reaction to occur. These spatial aspects of biodegradation in soils, including reactant mixing, have been the subject of a wide body of literature. However, the primarily focus has been on the saturated zone due to the relative simplicity and stability of saturated zone flow (e.g. Puyguiraud et al., 2020; Rolle & Le Borgne, 2019; Valocchi et al., 2019; Benson et al., 2017).

Monocomponent biodegradation processes, such as the widely studied first-order decay kinetics, are completely rate-limited. However, multicomponent biodegradation outcomes are governed by the rate of the reaction and the rate of mixing between reactants (e.g. Hesse et al., 2009; Battiato et al., 2009). The extents of these limitations affect the sensitivity of biodegradation outcomes to other model parameters (e.g. Song and Seagren, 2008 for saturated porous media). Furthermore, the extent of rate-limitation and mixing-limitation are not mutually exclusive (Bauer et al., 2008; Luo et al., 2008). This is because reactant concentrations, the biodegradation rate, and the rate of dispersion and mixing are mutually dependent. Therefore, aside from monocomponent

* Corresponding author.
E-mail address: darrell.tang@wur.nl (D.W.S. Tang).

https://doi.org/10.1016/j.jhydrol.2024.131111
Received 28 December 2023; Received in revised form 28 February 2024; Accepted 11 March 2024
Available online 29 March 2024

reactions, all biodegradation reactions are mixing-limited to some extent.

A factor that affects mixing and multicomponent biodegradation is the spatial variability of soil hydraulic properties and the flow field. In groundwater aquifers, it has been recognised that soil heterogeneity leads to increased mixing between incoming contaminant plumes and the groundwater (e.g. Rolle et al., 2009). Soil heterogeneity also leads to preferential flow (Gouet-Kaplan et al., 2012), which can increase flow velocities, decrease contaminant residence times, and reduce contaminant biodegradation. These studies considered either the saturated zone, where heterogeneity and transient flow have different implications, or monocomponent biodegradation, and are thus not fully applicable to multicomponent biodegradation in the unsaturated zone. Studies of multicomponent biodegradation in the unsaturated zone have usually considered one-dimensional columns with homogeneous soils (e.g. de Wilde et al., 2009; Barrios et al., 2019), where spatially explicit details of important transport processes such as preferential flow cannot be accurately reproduced due to the nature of one-dimensional space.

Transient flow, which is the general state of affairs in the unsaturated zone, also affects contaminant biodegradation. Relative changes in flow rates over time tend to be more frequent and larger in the unsaturated zone, because the unsaturated zone is exposed to atmospheric forcing, and because the hydraulic properties of soils (e.g. saturation and hydraulic conductivity) are dynamic under transient flow. Given that biogeochemical reaction rates are nonlinear with respect to reactant concentrations (Barry et al., 2002), and that water and solute fluxes are nonlinear with respect to time (Batalha et al., 2018; Schotanus et al., 2013), transient flow has the potential to affect biodegradation outcomes. Whether transient flow increases or decreases contaminant leaching relative to steady flow, and whether this effect is large, appears to be scenario-dependent, as no general conclusion can be made from the relevant literature (e.g. Schotanus et al., 2013; Yuan et al., 2011; Corwin et al., 2007; Kuntz & Grathwohl, 2009; Sander & Braddock, 2005).

Above, we have briefly described how multicomponent biodegradation (as opposed to monocomponent biodegradation), soil heterogeneity, and tranisent flow, may individually affect contaminant biodegradation outcomes in the unsaturated zone. However, when these processes occur simultaneously, interactions between these processes also give rise to higher-order complexity that affects biodegradation outcomes. In heterogeneous soils under unsaturated conditions, preferential flow and stagnant flow zones may swap positions when large changes in mean flow rates occur (Roth, 1995). When this occurs, reactants that infiltrate into the soil separately at different times are able to mix through transverse dispersion (see Fig. 1 for an illustration). In contrast, only longitudinal dispersion is possible in such a scenario in homogeneous soils where transport is characterized by one-dimensional behavior. Thus, preferential flow and stagnant flow zones will vary spatiotemporally. This dynamically changes the spatial distribution of reactants, the extent of reactant mixing, and the spatial overlap between contaminants and the contaminant-degrading microbes. Furthermore, in heterogeneous soils, dynamic compression and expansion of solute plumes due to pressure transmission (Warrick et al., 1971) can occur simultaneously in different regions of the soil. These processes, which affect mixing and hence also multicomponent biodegradation, can only occur in the simultaneous presence of both transient flow and soil heterogeneity.

In light of the above interaction-derived phenomena, it is our objective to study microbe-facilitated multicomponent biodegradation of soil contaminants, in scenarios where dynamic preferential flow arises from transient flow and soil heterogeneity. As far as we are aware, this combination of processes has not yet been studied in the literature. Scenarios with a large and discrete flow rate transition (low frequency, large amplitude variability) are particularly interesting as interaction effects between soil heterogeneity and transient flow are strong, resulting in a large extent of dynamic switching in the spatial locations

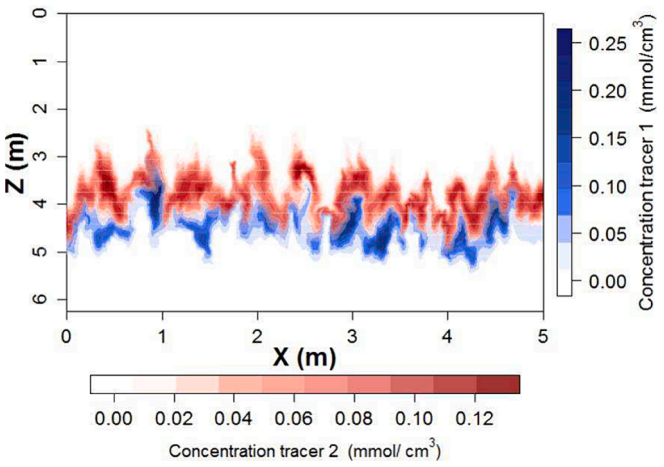

Fig. 1. Illustration of tracer plumes in a heterogeneous soil, which shows how two different tracers, which infiltrate into the soil sequentially, are able to mix through transverse dispersion in heterogeneous soils. The interface between the two tracers would be perfectly horizontal in a homogeneous soil, and no transverse dispersion would be possible. Reproduced with permission from de Vries (2016), who performed numerical simulations of non-reactive solute transport under transient flow in heterogeneous soils.

of preferential flow zones (Roth, 1995). Preferential flow zone switching does not occur to such a significant degree under typical weather fluctuations (high frequency, small amplitude variability). Therefore, in this study we specifically study transient flow scenarios with a large and discrete transition in flow rate, but not small amplitude variations in precipitation rate.

Cirpka and Valocchi (2007) analytically studied transversal mixing for homogeneous steady flow, and suggested that extending the model to transient flow or heterogeneous soils requires numerical modelling, due to its complexity. Therefore, in this study, where we incorporate both of these processes, we numerically model multicomponent biodegradation of infiltrating contaminants in a heterogeneous soil under transient flow. A realistic example of a scenario with a large and discrete flow rate transition is snowmelt-driven leaching of biodegradable contaminants through the soil. Other examples of large and discrete infiltration rate transitions include fluvial flooding, distinct seasonality effects such as in monsoonal climates, and cases where a large rainfall season follows a dryer season during which an agricultural field is irrigated.

2. Methods

2.1. Scenario development and background information: Biodegradable contaminant leaching under snowmelt conditions

De-icing fluids, such as propylene glycol, are transported from airport tarmacs to surrounding soils by surface runoff and mechanical snow removal (French et al., 2001; Pressl et al., 2019; Rodziewicz et al., 2020). They then slowly and gradually infiltrate into the soil, where they remain close to the topsoil for the rest of the season due to low infiltration fluxes. Upon snowmelt at the onset of spring, the infiltration rate instantaneously increases to levels that greatly exceed that before snowmelt (French et al., 2023; French et al., 2001). Soil pollution by de-icing fluids at Oslo Gardemoen airport in Norway, for example, is a concerning environmental issue that has been the subject of a substantial body of scientific literature (French et al., 2023). Across the various transient flow scenarios (L,M,H,E) that will be simulated in this study (Table 1), a cumulative infiltration of 115 cm takes place in 7 to 70 days, representative of the range of various snowmelt conditions observed at Oslo airport (French et al., 1999). The low infiltration rate scenario (L) with 1.00E-6 cm/s is similar to the annual average groundwater

Table 1
List of parameters and modelled scenarios. In the manuscript, scenario names such as "B1 with infiltration regime LH" imply that the biogeochemical reaction parameters are defined as in biodegradation rate scenario B and electron acceptor concentration scenario 1, while the infiltration regime is infiltration rate L before the flow rate transition, and infiltration rate H after the flow rate transition.

Infiltration rates	Explanation
L	1.00E-6 cm/s
M	1.09E-5 cm/s
H	1.00E-4 cm/s
E	1.00E-3 cm/s

Infiltration regime	Explanation
LH	Transient flow, slow to fast
LE	Transient flow, slow to very fast
MM	Steady-state flow
MH	Transient flow, medium slow to fast
ME	Transient flow, medium slow to very fast

Contaminant input concentration C_0	Explanation
2.5E-7 mol/cm^3	$C_0 \ll K_{A,C}$. The reaction begins in the first-order regime of the Monod rate curve.
2.5E-6 mol/cm^3	$C_0 \ K_{A,C}$. The reaction begins in the transition regime of the Monod rate curve.
2.5E-5 mol/cm^3	$C_0 \gg K_{A,C}$. The reaction begins in the zeroth-order regime of the Monod rate curve.

Electron acceptor concentration scenario	Explanation
1	Initial soil electron acceptor concentration = 0
2	Initial soil electron acceptor concentration $=2C_0$

Biodegradation rate scenario	Explanation
A	B_0= 8.75E-7 mol/cm^3 and $\mu = 6E\text{-}7\ s^{-1}$. Same initial reaction rate (equation (1) as scenario B; biomass grows relatively slow.
B	B_0= 8.75E-8 mol/cm^3 and $\mu = 6E\text{-}6\ s^{-1}$. Same initial reaction rate (equation (1) as scenario A; biomass grows relatively fast.
C	B_0= 8.75E-7 mol/cm^3 and $\mu = 6E\text{-}6\ s^{-1}$.

Parameter	Explanation	Value
θ_r	Residual soil water content	0.057 cm^3/cm^3
θ_s	Saturated soil water content	0.41 cm^3/cm^3
K_s^*	Reference saturated hydraulic conductivity	4.05E-3 cm/s
$\langle \log_{10}\lambda \rangle$	Mean of log(scaling factor)	0
$\sigma(\log_{10}\lambda)$	Standard deviation of log (scaling factor)	0.75
l_x	Horizontal autocorrelation length	20 cm
l_z	Vertical autocorrelation length	5 cm
α_v	Van Genuchten-Mualem parameter	0.124 cm^{-1}
n	Van Genuchten-Mualem parameter	2.28

(*continued on next page*)

Table 1 (*continued*)

Parameter	Explanation	Value
L	Van Genuchten-Mualem parameter	0.5
α_L	Longitudinal dispersivity	1 cm
α_T	Transverse dispersivity	0.1 cm
$D_{e,C}$	Diffusion coefficient (contaminant)	1.00E-5 cm^2/s
$D_{e,A}$	Diffusion coefficient (electron acceptor)	2.29E-5 cm^2/s
K_A	Electron acceptor half-saturation constant	5E-8 mol/cm^3
$K_{A,C}$	Half-saturation constant	1.25E-6 mol/cm^3
F	A : C stoichiometric coefficient	4
G	Biomass yield ratio	0.5
A_0	Initial electron acceptor concentration	Varies by scenario, see above
B_0	Initial biomass concentration	Varies by scenario, see above
C_0	Infiltrating contaminant concentration	Varies by scenario, see above
μ	Biodegradation rate constant	Varies by scenario, see above

recharge rate. At Oslo airport, the data suggests a field scale maximum daily infiltration rate of around 1.00E-4 cm/s (H), and a weekly average of around 1.00E-5 cm/s (M) during the week with most snowmelt (French & Binley, 2004). Instantaneous infiltration rates at specific spatial locations in the field could be larger than this; rates around 1.00E-3 cm/s (E) have been observed in other studies (Gray et al., 2001). Aside from the example of the leaching of deicing fluid, the infiltration rates simulated (Table 1) span a range from light rainfall events (1.00E-6 cm/s) to fluvial flooding (1.00E-3 cm/s).

Although aerobic biodegradation rates are typically much faster than anaerobic biodegradation rates, the importance of anaerobic biodegradation in removing contaminants from the environment is frequently underestimated (Hunter et al., 1998). This is especially true under snowmelt driven contaminant transport. Under ice cover during the winter, the replenishment of soil oxygen from the atmosphere is cut off (Kirillin et al., 2012), yet nitrification processes that deplete soil oxygen continue to occur (Voigt et al., 2020). Furthermore, a significant amount of the oxygen in the soil may be depleted through reactions with the inorganic byproducts of anaerobic biodegradation (Hunter et al., 1998). Even for microbe-contaminant combinations that may partake in aerobic biodegradation, anaerobic instead of aerobic biodegradation occurs if the oxygen concentration is below some threshold value (Barry et al., 2002). Therefore, in this study, we focus on the mixing of aqueous phase reactants and solid phase immobile microbial biomass, while assuming that aerobic biodegradation and vapor phase reactant transport are negligible. Omitting aerobic biodegradation allows us to ignore vapor phase oxygen diffusion through the soil, which would add yet another layer of complication to this already highly complex problem, and would be better placed in a follow-up study. In the anaerobic biodegradation of propylene glycol, the contaminant and participating electron acceptors (e.g. nitrate, sulphate) are all primarily transported in the aqueous phase (Mayer et al., 2002).

2.2. Transport and biodegradation model

The numerical simulations in this study concern Monod biodegradation of solutes in water that infiltrates into two-dimensional heterogeneous soils. The transport simulations were performed with HYDRUS2D (Šimůnek et al., 2012b), and the biogeochemical reactions were performed with PHREEQC (Parkhurst & Appelo, 2013). These two models are integrated in the HP2 biogeochemical reactive transport package (Šimůnek et al., 2012a). For comparison, scenarios with homogeneous soils instead of heterogeneous soils, but otherwise identical parameter values, were modelled with HP1 (Šimůnek et al., 2013), the one-dimensional version of HP2.

In HYDRUS2D, we discretized a 100 cm wide and 100 cm deep domain with a finite element mesh of 101 × 101 evenly spaced nodes. The soil-hydraulic van Genuchten-Mualem functions are used to characterize soil–water retention and the unsaturated hydraulic conductivity functions of soil. This provided a balance between model resolution and computational speed. The soil type is loamy sand in the entire domain, and the associated soil hydraulic parameters are obtained from Carsel and Parrish (1988). To model heterogeneous soils, random scaling of soil hydraulic parameters is generated in HYDRUS2D, using Miller-Miller similitude (Miller and Miller, 1956). Under Miller-Miller similitude, the pressure head and hydraulic conductivity at a certain soil water content are scaled according to a scaling factor, which we randomly generate using an exponential spatial autocorrelation (see Table 1 for statistical parameters). By using a longer horizontal than vertical autocorrelation length in generating the heterogeneous soil, we take into account the tendency for soils to be somewhat horizontally layered (e.g. Vereecken et al., 2007; Pedretti et al., 2013; Yu & Michael, 2022). For all scenarios, (the same) 12 realizations of the heterogeneous scaling factor field were simulated, in addition to the homogeneous case. Unless stated otherwise, results reported for heterogeneous soils refer to averaged outcomes. Table 1 lists the soil hydraulic parameter values and statistical distributions of soil heterogeneity used in the simulations.

Anaerobic biodegradation is modelled with Monod kinetics as described by Barry et al. (2002). A generic formulation of biodegradation reaction rates under Monod kinetics is

$$\frac{dC}{dt} = -\mu \frac{A}{k_A + A} \frac{C}{k_{A,C} + C} B \tag{1}$$

$$\frac{dA}{dt} = F \frac{dC}{dt} \tag{2}$$

while eliminated contaminant is converted to biomass at the following rate

$$\frac{dB}{dt} = -G\frac{dC}{dt} \quad (3)$$

Here, A and C [mol/cm^3 water], and B [mol/cm^3 soil] are the electron acceptor, contaminant, and biomass concentrations respectively. μ [s^{-1}] is the biodegradation rate constant, k_A [mol/L water] is the half-saturation constant of the electron acceptor, $k_{A,C}$ [mol/L water] is the half-saturation constant for the redox reaction between the electron acceptor and contaminant, F is the stoichiometric ratio of the electron acceptor in the biodegradation reaction relative to the contaminant, and G is the dimensionless yield ratio for biomass growth. We omit biomass movement from the model, as it may be assumed negligible (e.g. Holden and Fierer, (2005); Grösbacher et al., (2018)). We also assume a uniform initial biomass concentration, and uniformly zero contaminant concentration, in the entire model domain.

A free drainage and boundary condition for water flow is used at the bottom of the domain, signifying that the water table is sufficiently deep that it does not affect hydraulic heads in the simulated domain. This is a simple and realistic lower boundary for the coarse glaciofluvial sediments in the example case of Oslo airport and the surrounding region, where the depth to groundwater ranges from 6 m (French et al., 2023) to over 100 m (Olsen et al., 2013). A prescribed flux boundary is used at the top of the domain, and no flow boundaries are used at the sides. The initial condition for moisture content in the soil is at steady-state with respect to the initial infiltration rate at the upper boundary, and the initial condition for contaminants is zero concentration everywhere. Simulations begin with the soil containing a spatially uniform distribution of biomass (active in biodegradation) and electron acceptor.

The simulated transient flow scenarios involve a single flow rate transition, where slow infiltration of contaminant-carrying water is followed by a sudden and fast influx of contaminant-free water. Here, the slow infiltration period represents the gradual infiltration of contaminants during the winter, while the fast infiltration period represents snowmelt at the end of the winter season. At transition, the infiltration rate changes instantaneously to a new value, occurring approximately when the center of the contaminant plume is at a depth of 35 cm. This transition time, and the total infiltrated contaminant mass, is identical for all scenarios with the same pre-transition infiltration rate. For steady-state scenarios, the post- and pre-transition infiltration rates are identical. All post-transition infiltrated water is contaminant-free water containing dissolved electron acceptors, at the same concentration as initially present in the contaminant band. The simulations continue until the cumulative post-transition infiltration is 100 cm of water (before correcting for porosity and saturation), upon which the simulations terminate.

Parameters describing the biodegradation reaction are realistic values for propylene glycol, a biodegradable contaminant that exhibits minimal retardation in the soil (Schotanus et al., 2014). We simulate various biogeochemical scenarios, to investigate how they interact with the combination of complex processes we model. Table 1 lists the various scenarios and their parameter values, which are simulated for all possible combinations. Simulating different combinations of the biodegradation rate constant μ and the initial biomass concentration B_0 allows us to keep the initial biodegradation rate identical across multiple scenarios, while changing the relative rate of biomass growth (i.e., the relative biomass growth rate is faster when B_0 is smaller). This would elucidate the influence of biodegradation rate increases due to biomass growth. We also varied the contaminant concentration while keeping the electron acceptor:contaminant ratio constant. This enables us to compare the impact of starting at the almost linear (first-order) or at the plateau (zeroth-order) part of the nonlinear Monod rate curve. We also compare scenarios with initially high and low soil concentrations of electron acceptors, as these scenarios are affected differently by mixing. The biomass is assumed to not decay over time, under the assumption that the time scale of biomass decay is much larger than the timescale of transporting a solute plume 1 m into the soil. Furthermore, effects of biomass concentrations on contaminant fate may be observed by comparing scenarios A,B,C (Table 1). Additional simulations with first-order monocomponent biodegradation with a constant decay rate 6E-7 s^{-1}, and where biomass growth is tracked but not factored into the decay rate, are also performed. These first-order simulations are presented for comparison where appropriate, but excluded from the general data analyses.

2.3. Analysis of contaminant fate

The primary outcomes analyzed are the biodegraded fraction F_d and the spatial distribution of biomass growth $B(x, z)$. Since the modelled biomass is immobile and does not decay, $B(x, z)$ is a cumulative snapshot of where contaminant is biodegraded and reaction byproducts are formed. In turn, this contains spatial information about mixing and biodegradation. The leached fraction $L_d = 1 - F_d$ is the fraction of infiltrating solutes that exit the bottom of the soil column.

We attempted to investigate whether an easily observable modified form of the Damköhler number Da, may be used to characterize biodegradation outcomes. The original Damköhler number Da_0 specifies the dimensionless ratio of the reaction rate over the characteristic transport (advection) rate of the system, and is widely used in describing and characterizing first-order biodegradation in hydrogeological systems (e.g. Kuntz and Grathwohl, 2009). The Damköhler number describes how much the biodegradation is limited by reaction rate, relative to the transport velocity. A large Damköhler number would imply that more contaminants are biodegraded and less are leached, and vice-versa. In the idealized case that biodegradation is first-order, soils are homogeneous, and no dispersion occurs, F_d and the Damköhler number are related exactly through the relationship $F_d = 1 - \exp(-Da_0)$. For multicomponent Monod kinetics, the Damköhler number is ill-defined, as there is no constant biodegradation rate. Therefore, we introduce a modified version of the Damköhler number, Da, that may be more easily determined in field and laboratory situations. This modified Damköhler number may possibly be used to roughly estimate or characterize biodegradation outcomes such as F_d, which is more difficult to measure. We define this modified Damköhler number as $Da = \frac{t_{peak}}{C_0}\left(\frac{dC}{dt}\right)_{t=0}$, where t_{peak} is the time at which the peak of the contaminant plume exits the soil column, and $\left(\frac{dC}{dt}\right)_{t=0}$ is easily calculated from equation (1), given that initial reactant concentrations at the soil surface upon infiltration are known.

3. Results and discussion

3.1. Flow and transport

The locations of preferential flow zones, and the extent to which they conduct water faster than the average, depend upon the infiltration rate (Fig. 2). Briefly explained, the fine grained regions of soil are more hydraulically conductive than the coarse grained regions under dryer conditions as flow occurs primarily through capillary forces. On the other hand, the coarse grained regions are more conductive under wetter conditions as flow occurs mostly by gravity (see Roth (1995) for a detailed mechanistic explanation of this phenomenon). As the infiltration rate increases from rate L (1.00E-6 cm/s) to rate H (1.00E-4 cm/s), preferential flow becomes less dominating. This is because the flow finger becomes wider and the maximum flux in the preferential flow channel decreases from around 20I to 3I, where I is the dimensionless vertical component of flow velocity divided by infiltration rate (Fig. 2). When the infiltration rate increases further from rate H (1.00E-4 cm/s) to rate E (1.00E-3 cm/s), the preferential and stagnant flow zones also switch in spatial location, in addition to changing in magnitude (Fig. 2). The extent of differentiation in the magnitudes of I between preferential and stagnant flow zones is the largest, and the extent of solute plume deformation relative to a homogeneous soil is largest, for low infiltration

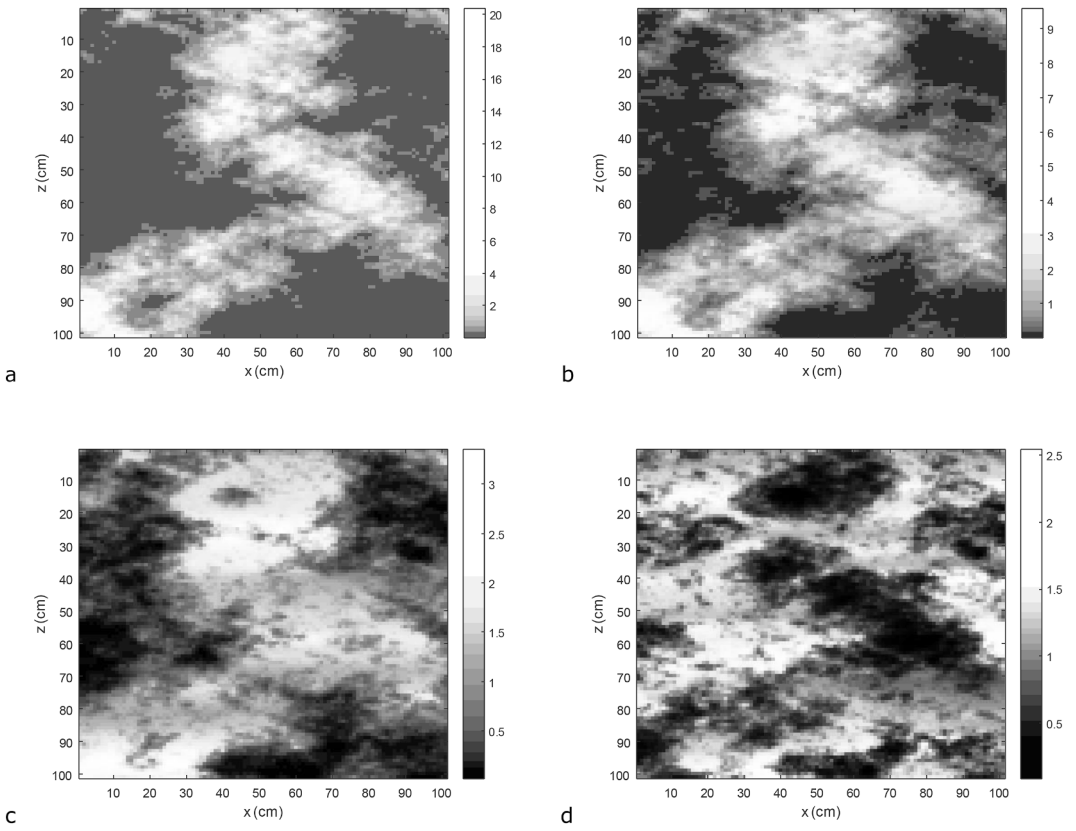

Fig. 2. Maps of the vertical component of flow velocity divided by the infiltration rate, a dimensionless ratio, in one realization of the heterogeneous soil, for infiltration rates (a) L, (b) M, (c) H, (d) E (see Table 1 for infiltration rate values) respectively at steady-state.

rates. This is in agreement with Ursino et al. (2001), and Schotanus et al (2012) and (2013).

We use the time at which the peak of the contaminant plume exits the soil column, t_{peak}, as an approximation for quantifying the mean residence time of contaminant particles, for several reasons. Firstly, the breakthrough curves at the outlet (averaged across the horizontal dimension) were found to be approximately Gaussian for all scenarios, regardless of whether the soil is homogeneous or heterogeneous, as illustrated in the examples in Fig. 3. This implies that the peak does indeed approximate the mean residence time of contaminant particles that escape biodegradation. Secondly, t_{peak} is relatively easily to observe in the field, and contains some predictive information value on the fraction of contaminants leaching to groundwater (Section 3.2).

Fig. 3a shows an example scenario where leaching times are on average much earlier in a heterogeneous soil than in a homogeneous soil under steady state flow. Fig. 3b shows that the same applies under transient flow, but the difference is smaller. Indeed, for 83 out of the 90 Monod biodegradation scenarios, t_{peak} of the contaminant peak arrived earlier in the heterogeneous scenarios than in the homogeneous scenarios. In the remaining 7 scenarios, t_{peak} in heterogeneous soils was earlier, but by no more than 0.1 %, compared to homogeneous soils (see Supplementary Material for data). In steady-state scenarios in particular, t_{peak} is on average 14 % smaller, and up to 21 % smaller in a heterogeneous realization than in homogeneous soils. This suggests that the persistent preferential flow in heterogeneous soils are able to quickly channel much of the contaminant plume to the bottom of the soil column; this point will be discussed further in Section 3.4. This confirms that heterogeneity reduces the mean travel time under steady-state flow (Birkholzer and Tsang, 1997), by focusing the transport of solutes within preferential flow channels. For all transient flow scenarios, any reduction in t_{peak} due to heterogeneity is less than 2 percent, because preferential flow zone switching in heterogeneous soils causes each part of the solute plume to spend some time in a preferential flow zone and some time in a stagnant flow zone. For the same reason, very little solute mass remains trapped in stagnant flow zones in transient flow scenarios (Fig. 1). Therefore, we emphasize that heterogeneity mostly decreases leaching times. Hence, if more total biodegradation occurs in a heterogeneous soil than in a homogeneous soil, it must be attributed to enhanced mixing, not because of prolonged time for degradation or contaminants being trapped in stagnant flow zones (especially under transient flow).

3.2. *Effects of biogeochemical parameters on contaminant fate*

The complete list of F_d of all the simulated scenarios (averaged from the twelve heterogeneous realizations) is given in the Supplementary Material. Comparing F_d data of all scenarios shows that overall F_d depends much more significantly on the infiltration rates and biogeochemical parameters, than on whether soil heterogeneity was simulated.

For most scenarios, the biodegraded fraction depended significantly on the initial soil electron acceptor concentration, but was quite insensitive to the relative initial biomass growth rate. This reveals a bottleneck behavior based on either biomass or electron acceptor as a limiting reagent: each scenario is highly sensitive to either initial electron acceptor concentration or biomass growth rate, but never both or neither. When electron acceptor availability is the limiting factor, a larger biomass growth rate only shifts biomass growth (i.e., the location where biodegradation occurs) to shallower soil, but does not increase total biodegradation. The few scenarios where the initial biomass growth rate is the significant limiting factor occur when the pre-transition infiltration rate is medium (M) instead of low (L), and large reactant concentrations are present in the infiltrating contaminant plume. This shows that the relative biomass growth rate is more important when the infiltration rate is relatively fast and the

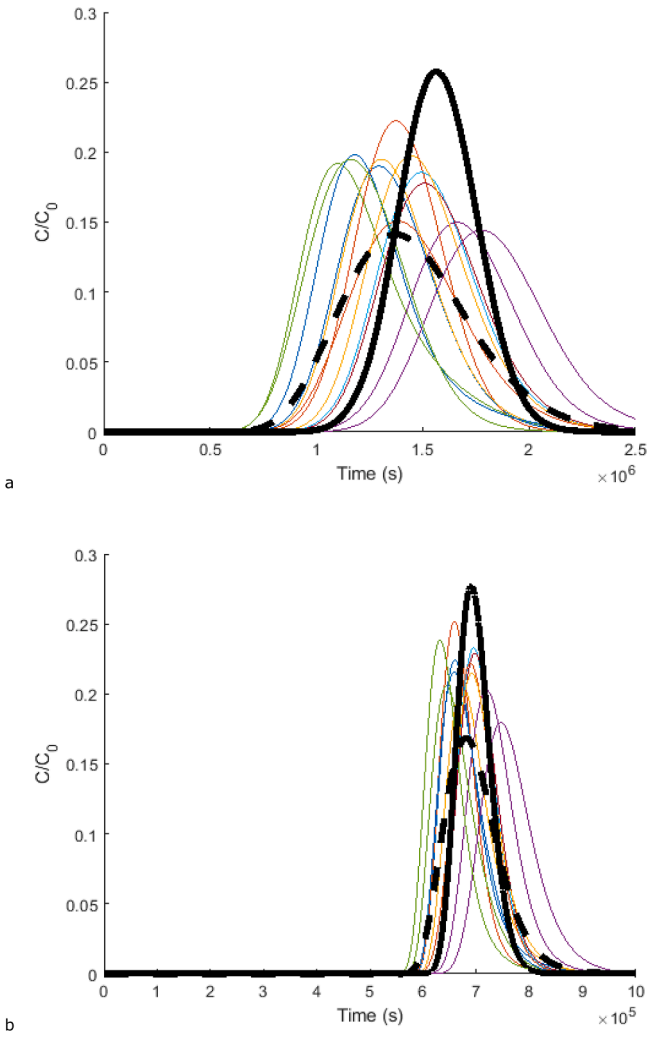

Fig. 3. Breakthrough curves for all 12 realizations of the heterogeneous soil, the heterogeneous average (bold dashed line), and the homogeneous soil (bold solid line), for (a) MM (steady-state flow) and (b) MH (transient flow) infiltration scenarios respectively, for scenario C1 with contaminant input $C_0 \gg K_{A,C}$.

contaminant itself is not a limiting reagent for the biodegradation reaction. The reason is that in such cases, the contaminant plume is more quickly advected away from established biomass hotspots.

When varying the infiltrating contaminant concentration C_0 in Monod biodegradation scenarios, the highest degraded fraction occurs when C_0 is similar in magnitude to the half-saturation constant $K_{A,C}$ (i.e., C_0 $K_{A,C}$). Therefore F_d varies non-monotonically with C_0, and this can be analytically proven for a perfectly mixed reaction. Consider two generic perfectly mixed Monod biodegradation scenarios with $C_0 = C_1$ and $C_0 = C_2$, where $C_1 < C_2$ and $C_1, C_2 \ll K_{A,C}$. This reaction behaves similarly to first-order decay with growing rate constant. To illustrate, we omit the electron acceptor concentration dependence, and absorb the biomass term into the rate constant $\mu'(t) = \mu B(t)$, so that $\frac{\partial C}{\partial t} \approx -\mu BC = -\mu'(t)C$. Since $C_1 < C_2$, it follows that $\left(\frac{\partial B}{\partial t}\right)_1 < \left(\frac{\partial B}{\partial t}\right)_2$, $B_1(t) < B_2(t)$ and $\mu_1'(t) < \mu_2'(t)$ for all $t > 0$, ultimately resulting in $F_{d,1} < F_{d,2}$. Now instead consider the cases $C_0 = C_3$ and $C_0 = C_4$, where $C_3 < C_4$ and $C_3, C_4 \gg K_{A,C}$. For all small t (i.e., while the reaction remains zeroth-order), $B_1(t) \approx B_2(t)$ and $\left(\frac{\partial C}{\partial t}\right)_3 \approx \left(\frac{\partial C}{\partial t}\right)_4$. Therefore, $\frac{d}{dt}\left(\frac{C}{C_0}\right)_3 > \frac{d}{dt}\left(\frac{C}{C_0}\right)_4$ and $F_{d,3} > F_{d,4}$. Therefore, F_d for Monod kinetics varies non-monotonically with C_0, showing a maximum approximately when C_0 $K_{A,C}$. Amongst the scenarios we simulated, F_d varies non-monotonoically with C_0 for 53 % of Monod scenarios. The non-monotonicity is not observed in all simulated scenarios, because the assumption of perfect mixing does not hold. This emphasizes the importance of considering mixing in determining the fate of contaminants in our scenarios.

A scatterplot of F_d against the modified Da for all simulated scenarios (Fig. 4a) shows that this theoretical relationship does not describe the studied scenarios well. The equation $F_d = 1 - \exp(-Da)$ appears to be a lower bound for $\log_{10}(Da) < -1$ and upper bound for $\log_{10}(Da) > 1$. Remarkably, the data in Fig. 4a shows that F_d clusters around the shifted curve F_d $1 - \exp(-\beta Da)$, where β is an empirical constant. In other words, the data appears to be explained well on average through an analysis of the Damköhler number if the Damköhler number was multiplied by an empirical factor β, which appears to be around 10 for the scenarios we have simulated (Fig. 4a). For illustrative purposes, this information is also presented in terms of the leached fraction $L_d = 1 - F_d$ in Fig. 4b. This means that although the modified Damköhler number does not have much standalone prediction value for such complex scenarios, it is able to roughly predict the relative mean sensitivity of F_d and L_d to local changes in parameter space.

From Fig. 4a and b, it is evident that the semi-analytical expressions F_d $1 - \exp(-\beta Da)$ and L_d $\exp(-\beta Da)$ are much more accurate at low Da (i.e., $\log_{10}(Da) < -0.5$). A value of β around 10 describes the scenarios with $\log_{10}(Da) < -0.5$ very well; the spread in data around the fitted line is within ± 0.5 on the $\log_{10}(Da)$ axis. The empirical factor β captures the effects of processes not included in the Damköhler number. Two important aspects of contaminant transport are not captured in the computation of Da: 1) biomass growth, reactant spreading, and mixing between the reactants and biomass, and 2) any inadequacies of using the observed t_{peak} of a biodegradable plume as a proxy for characterizing solute residence times in the soil column. Additional runs of the simulations in Table 1 with inert tracers (not shown) reveal that t_{peak} is always larger for tracers than biodegrading solutes. Hence, if aspect 2 above was dominant, contaminant residence times in the soil column would be underestimated if t_{peak} was calculated from observations of a biodegradable plume, resulting an empirically fitted β value smaller than 1. As aspect 1 is the only process not considered in the Damköhler number that could increase β substantially, the fact that the fitted β is much larger than 1 suggests that aspect 1 is dominant. This in turn suggests the key role of biomass growth, reactant spreading, and reactant mixing, in determining solute fate. By extension, this indicates the importance of soil heterogeneity in determining reactant mixing and contaminant fate, which we explore further in Section 3.3. The fact that the data clusters without obvious systematic bias around F_d $1 - \exp(-\beta Da)$ and L_d $\exp(-\beta Da)$ at low Da suggests that β captures the main effects of aspect 1, and that the residual effects not captured in Da and β, combine to yield a random perturbation on biodegradation outcomes.

Fig. 4a and b show that when the relative rate of biomass growth (compare blue and red markers for biodegradation scenario A and B) is varied, which is not captured within Da, the cloud of points shift upwards or downwards. When parameters captured within Da are changed, such as the biodegradation rate constant (compare blue and magenta markers for biodegradation scenario A and C in Fig. 4a and b) or the initial concentration C_0 (Fig. 4c and d), the cloud of points move along the fitted F_d and L_d curves. Hence, the empirical equations F_d $1 - \exp(-\beta Da)$ and L_d $\exp(-\beta Da)$ can be analytically applied for approximate sensitivity analyses if parameters captured in Da are varied, once β is known. For illustration, we attempted to predict scenario A outcomes, using scenario C data and $L_d = \exp(-\beta Da)$, assuming it is known that β 10. The equation used for the prediction of $L_{d,A}$ is $L_{d,A} \approx L_{d,C} + \exp(-\beta Da_A) - \exp(-\beta Da_C)$, where subscripts A,C refer to the scenarios. The outcome (Fig. 4e) shows that the clouds of predicted (black) and actual (blue) outcomes overlapped each other and the empirical curve. The mean absolute error in predicting $L_{d,A}$ is 0.158, which may be accurate enough for coarse estimation purposes.

The analysis of the above paragraph also suggests that the empirical equations F_d $1 - \exp(-Da)$ and L_d $\exp(-Da)$ can be analytically applied

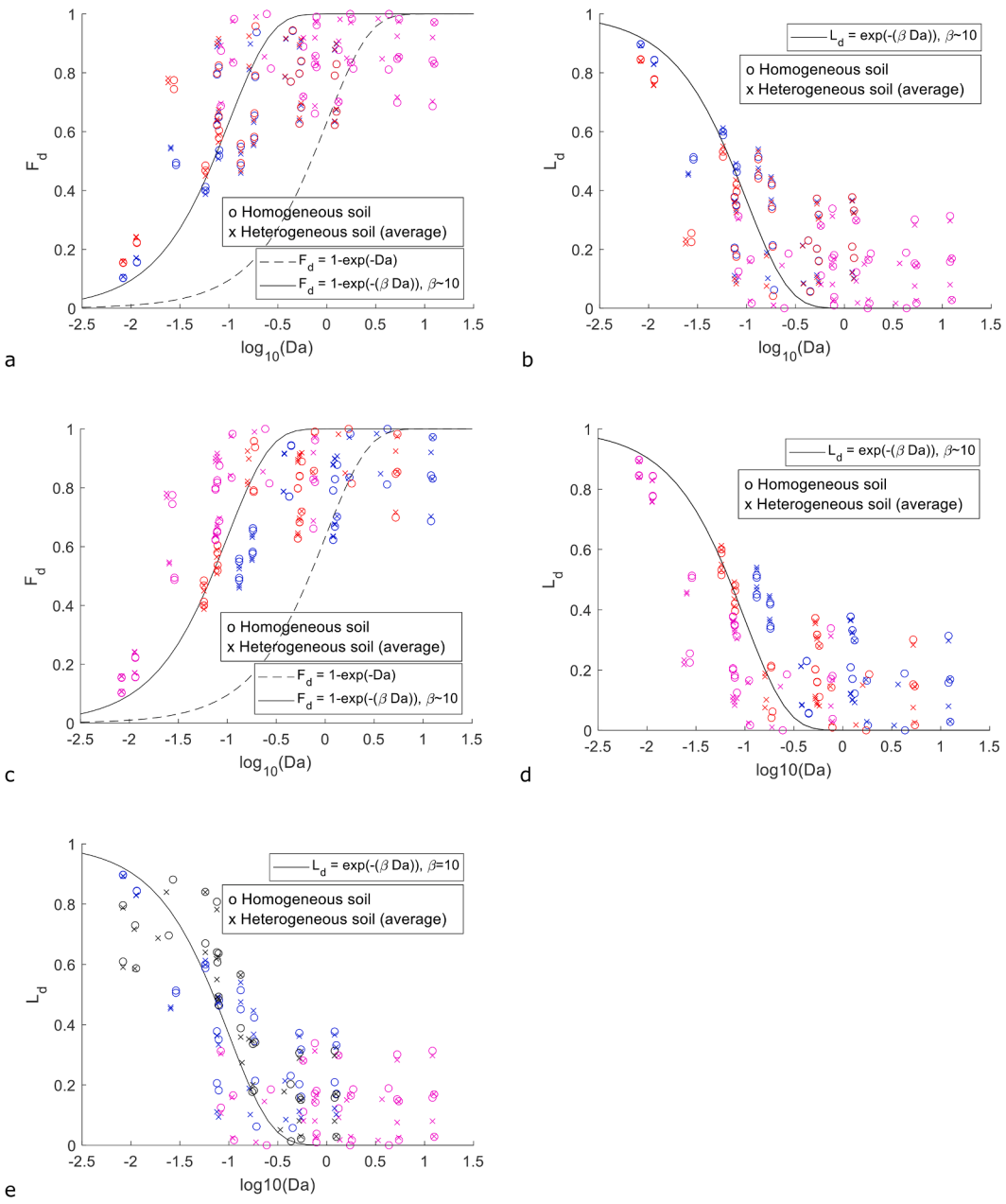

Fig. 4. First row: Scatter plot of a) F_d and b) L_d against $log_{10}Da$ for all scenarios, where blue, red and magenta refer to biodegradation scenario A, B, C respectively. Second row: Scatter plot of c) F_d and d) L_d against $log_{10}Da$ for all scenarios, where blue, red and magenta refer to contaminant input scenario $C_0 \gg K_{A,C}$, C_0 $K_{A,C}$, $C_0 \ll K_{A,C}$ respectively. Third Row: e) Blue and magenta refer to simulation data for biodegradation scenario A and C respectively. Black markers are attempts to predict scenario A outcomes, by applying the Damköhler analysis (Section 3.2) to simulation data from scenario C. (For interpretation of the references to colour in this figure legend, the reader is referred to the web version of this article.)

for relative sensitivity analyses of leached outcomes if parameters captured in Da are varied, even if β is unknown. In other words, the relative leachability of contaminants under various scenarios can be ranked against other scenarios even if β is unknown, although the leached fractions cannot be quantitatively predicted. Therefore, we have distilled the highly complex problem and its associated high-dimensional parameter hyperspace into a relatively simple dimensionless analysis, that may be used for performing approximate local sensitivity analyses of leaching outcomes in a battery of related scenarios.

3.3. Role of mixing in biodegradation outcomes

A large body of literature shows that soil heterogeneity increases dispersion and mixing (Birkholzer & Tsang, 1997; Moreno & Tsang, 1994; Rolle et al., 2009; Valocchi et al., 2019; Cirpka et al., 2011; Luo et al., 2008; Willingham et al., 2010; Werth et al., 2006). Since we have found that soil heterogeneity led to either similar or decreased residence times in all scenarios, it follows that if F_d is increased by soil heterogeneity then the scenario is likely to be mixing-limited. Here, mixing-limited implies that an increase in mixing would appreciably increase the extent of biodegradation. In this section, we attempt to identify which scenarios are mixing-limited, and to provide physical explanations for the mixing-limitation, to facilitate the identification of mixing-limited scenarios in future research. Through this, it would become easier to decide when computationally intensive simulations, that take into account the complex processes that affect mixing, are necessary.

Out of 90 Monod scenarios, 59 were mixing-limited as F_d was larger in heterogeneous soils than in homogeneous soils. Scenarios are found to

be mixing-limited if one or more of the following three criteria are fulfilled. 1) The initial infiltration rate is low (regime L), which makes biodegradation less limited by reaction rate. 2) The incoming contaminant concentration is large ($C_0 \gg K_{A,C}$). This is because even as the contaminant plume grows due to dispersion, the reaction rate per unit soil volume does not decrease much, because it is in the zeroth-order (plateau) region of the Monod rate curve. Therefore, its biodegradation potential is limited by how fast the contaminant plume can spread and mix. The observations that a large C_0 and transport dominated by diffusion (i.e., low advection velocity) leads to enhanced biodegradation under spatially heterogeneous concentrations has also been made by Hubert et al (2020), for reactions in a bulk fluid. 3) The initial electron acceptor concentration is large and the initial infiltration rate is low. Then, the reaction is less rate-limited, as electron acceptors are abundant outside of the contaminant plume in this case, hence biodegradation is more sensitive to how much mixing occurs. An inspection of all three criteria presented here suggests that physically, mixing-limitation occurs when the velocity of advection is relatively slow (criterion 1), the timescale of the biodegradation reaction (criterion 2) is relatively large (due to the zeroth order behavior of the Monod rate curve if $C_0 \gg K_{A,C}$), and there are sufficient electron acceptors in the soil to mix with the contaminant plume (criterion 3), which enables dispersion (and mixing) to have relatively large impacts on biodegradation outcomes.

For each of the above three criteria, we give a score (0,1) which we sum up to obtain the total mixing-limitation score. This score reflects the extent that mixing is the dominant limiting factor. For a score of 0, biodegradation is limited predominantly by the reaction rate, whereas a score of 3 indicates strong mixing-limitation. Note that this is meant to be a qualitative score, and should be interpreted only in the sense that a larger score implies a reaction more limited by mixing. Therefore, we do not intend to imply that the extent of mixing-limitation is proportional to the score. These factors that contribute to the mixing-limitation score suggest that rate-limited biodegradation is more limited by the rate of consumption of electron acceptors initially present in the contaminant plume, while mixing-limited biodegradation is limited by the extent of spreading and mixing with electron acceptors external to the contaminant plume.

There are 36, 30, 18 and 6 scenarios with a mixing-limitation score of 0, 1, 2 and 3, respectively. The scenarios with a score of at least 1 overwhelmingly have F_d larger in heterogeneous soils than in homogeneous soils (Fig. 5a). The mean increase in F_d, compared to homogeneous soils, increased with the mixing-limitation score, and were −2%, 3 %, 6 % and 10 % respectively. The effects of heterogeneity in increasing biodegradation are significantly more substantial if quantified in terms of the leached fraction $L_d = 1 - F_d$ (Fig. 5b). The respective mean increases in L_d are 12 %, −3%, −24 %, and −55 %. Since the F_d ratio (Fig. 5a) increases on average with increasing mixing-limitation score, we have identified an important (non-exhaustive) set of scenario criteria that contributes towards mixing-limitation. Furthermore, the higher the mixing-limitation score, the less likely that heterogeneity decreases F_d of a scenario (Fig. 5a). The small average effect of heterogeneity on F_d for scenarios with a mixing-limitation score of 0 agrees with Mohamed et al. (2006), who found that soil heterogeneity has minimal impact on Monod F_d, in the limiting case where the contaminant and electron acceptors are already perfectly mixed upon entry into the soil (i.e., perfectly not mixing-limited).

The significant value of the mixing-limitation score in predicting the effects of heterogeneity on F_d is even more apparent when comparing Fig. 5a to c. Fig. 5c shows that the modified Damköhler number has essentially zero predictive power on the F_d ratio (heterogeneous F_d/homogeneous F_d). Nevertheless, an interesting nuance can be seen in Fig. 5c. Although Fig. 5c does not show a clear relation between the F_d ratio and Da, a weak positive relationship is evident for only the black-colored points, which represent scenarios with a mixing-limitation score of 0. This suggests that the F_d ratio increases for rate-limited scenarios when Da increases (i.e., when the extent of rate-limitation decreases). As

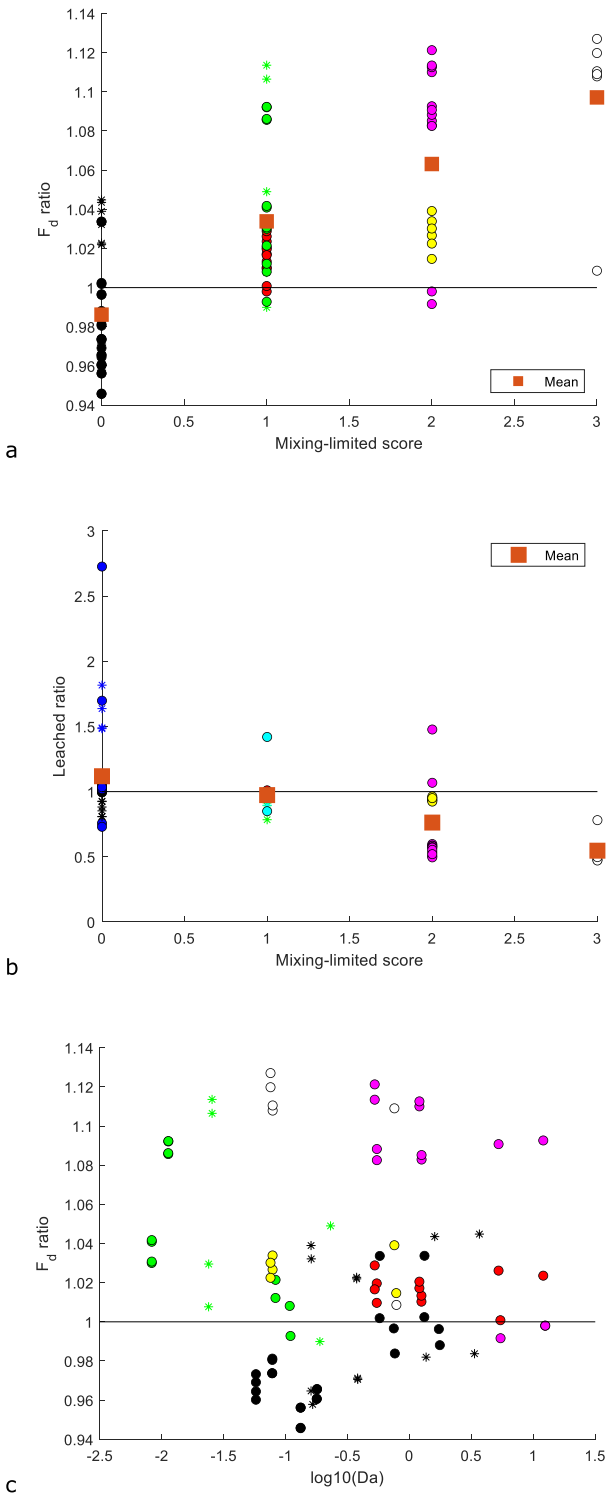

Fig. 5. Scatter plot of how the F_d ratio, $F_d(heterogeneous)/F_d(homogeneous)$ varies with a) mixing-limitation score and c) *Da*. A ratio larger than 1 implies that the heterogeneous average F_d is larger than the homogeneous case, and vice versa. Solid and asterisk symbols refer to transient and steady flow respectively. The colors represent combinations of mixing criteria 1, 2, and 3 (see section 3.3). Red = (1); Green = (2); Magenta = (1,3); Yellow = (1,2); White = (1,2,3); Black = rate-limited scenario. Fig. 5b shows the same information as Fig. 5a, but is presented in terms of the leached ratio $[1 - F_d(heterogeneous)]/[1 - F_d(homogeneous)]$. (For interpretation of the references to colour in this figure legend, the reader is referred to the web version of this article.)

rate-limitation becomes less dominant (i.e., Da increases), the fact that soil heterogeneity decrease contaminant residence times becomes less relevant. Therefore, soil heterogeneity is more likely to have negligible effects on F_d (leading to F_d ratios $\sim$ 1), or even positive effects on F_d (leading to F_d ratios $>$ 1 through increased mixing), when Da increases, even if the scenario-based mixing-limitation score is 0. Hence, rate-limitation and mixing-limitation are not mutually exclusive, as also discussed in Bauer et al. (2008), and may only be compared in terms of which is more dominant.

The results of our simulations also allow us to draw a general conclusion: that heterogeneity does not necessarily decrease the biodegraded fraction for multicomponent reactions, in particular for mixing-limited scenarios. We calculated the coefficient of variation of the biodegraded fraction across heterogeneous realizations, for all individual scenarios. We found that out of 90 scenarios, in only 9 cases did heterogeneity decrease the biodegraded fraction by a fraction larger than the coefficient of variation. Furthermore, out of the 54 scenarios with a mixing-limited score larger than 0, in only 1 scenario did heterogeneity decrease the biodegraded fraction by a fraction larger than the coefficient of variation. These results are in contrast to prior research that considered monocomponent biodegradation reactions (e.g., Beltman et al., 1995; van der Zee & Boesten, 1991; Jury & Gruber, 1989), which have attributed significantly larger risks of contaminant leaching in heterogeneous soils, on account of preferential flow. Further research with a wider range of scenarios, a larger set of soil heterogeneity statistics, and more simulated realizations for each heterogeneous soil, could perhaps strengthen this conclusion and reveal whether soil heterogeneity substantially contributes to increased contaminant

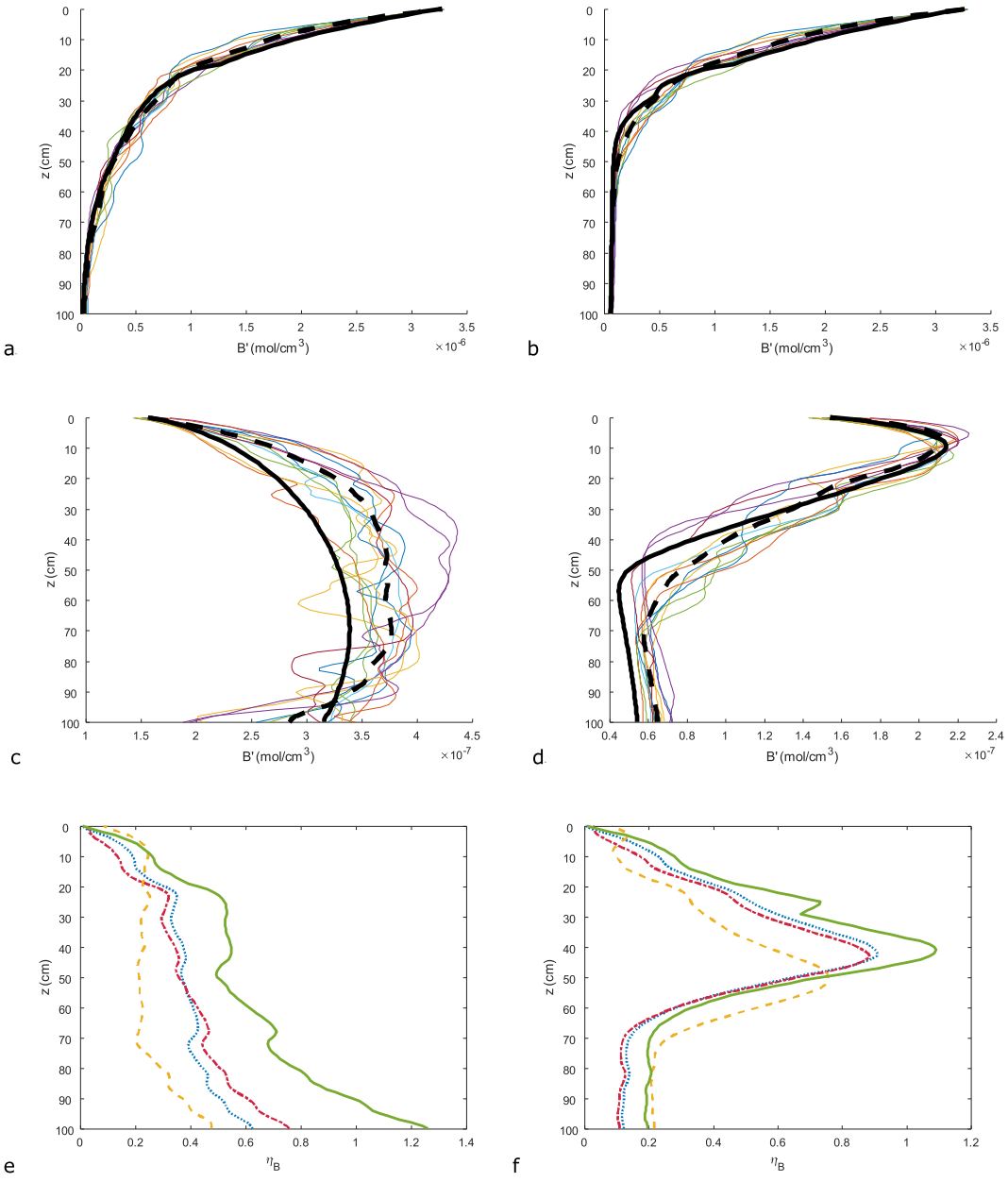

Fig. 6. Depth against biomass growth $B^{'} = B - B_0$. The bold solid line is for homogeneous soils, the bold dashed line is for the heterogeneous average, and the thin solid lines are for individual realizations in heterogeneous soils. (a,b) First-order biodegradation, steady-state MM and transient MH infiltration respectively. (c,d) Biodegradation rate scenario B1 and $C_0 \gg K_{A,C}$, with steady-state MM and transient MH infiltration respectively. (e,f) Depth against horizontal coefficient of variance of biomass η_B at the end of the simulation for Monod scenario B2, under (e) steady-state infiltration MM and (f) transient infiltration MH. The dashed, dotted, and dash-dotted lines are for Monod biodegradation with $C_0 \gg K_{A,C}$, $C_0 \ll K_{A,C}$, and $C_0 \ K_{A,C}$ respectively. The solid line represents a first-order biodegradation scenario.

biodegradation in practice.

3.4. Spatial distribution of microbial biomass

The resulting spatial distribution of biomass determines where and to what extent future influxes of contaminant will be biodegraded in the soil, and how the infiltration rate and its variability affect biodegradation. Under highly variable infiltration rates, contaminant infiltration paths during subsequent influxes may bypass established biomass hotspots if biomass is heterogeneously distributed in the soil. The spatial distribution of biomass also reveals the spatial distribution of reaction byproducts, especially immobile compounds, whose spatial distribution may be important as they may be (eco-)toxic. Furthermore, we show that the spatial distribution of biomass is affected by biodegradation kinetics, reactant mixing and subsurface flow patterns. The biomass distribution may therefore provide some information about these aspects, which are difficult to directly observe or measure in the field.

The simulations for the lowest initial infiltration rate (LH, LE) show that almost all of the biodegradation occurs in the uppermost layers. Thus, $\langle B(z)\rangle$ decays monotonically with depth for these scenarios, similar to experimentally observed $\langle B(z)\rangle$ (Biró et al., 2014) for first-order biodegradation. Fig. 6a (steady-state) and Fig. 6b (transient flow) illustrate simulated $\langle B(z)\rangle$ for first-order biodegradation. Unlike first-order biodegradation, for Monod kinetics a maximum in $\langle B(z)\rangle$ might occur some distance beneath the surface (Fig. 6c with steady-state flow, Fig. 6d with transient flow) under larger initial infiltration rates, regardless of steady-state or transient flow. We refer to this distance as the maximum biomass depth d_{max}.

In the scenarios where $\langle B(z)\rangle$ does not monotonically decrease with depth, the reason is that dispersion causes the contaminant and electron acceptor plumes to spread as the plume travels downwards. The initial decrease in reaction rate due to contaminant spreading and biodegradation is small. Hence, the biomass at d_{max} has greater total exposure time to the reaction, as compared to the top of the soil, due to the larger plume encountered. The biomass at d_{max} also encounters more backwards dispersion than the biomass at the topsoil. If the larger total exposure time outweighs the slow decrease in reaction rate, then soil at d_{max} will experience more total reaction than upstream soil. Therefore, Monod biodegradation activity is often largest at some depth beneath the soil surface, especially when reactants require time and distance to mix. On the other hand, first-order biodegradation activity is always at a maximum at the soil surface, as it is not mixing-dependent. Under field and experimental conditions, both monotonically decreasing and non-monotonically varying biomass densities have been observed (Hickman & Novak, 1989; Soulas and Lagacherie, 2001). This implies that the difference in outcomes between mixing-limited and rate-limited biodegradation scenarios is dependent on the thickness of the unsaturated soil column, which has to be sufficiently thick for reactants to mix fully under mixing-limited biodegradation, and should be investigated in more detail in future studies.

The vertical distribution of the biomass population varies significantly in shape between each heterogeneous realization, and the heterogeneous average (Fig. 6). However, the heterogeneous average $B(z)$ is similar to the homogeneous $B(z)$ in shape and (non–)monotonicity. Although the shape of the average $B(z)$ curve is similar in heterogeneous and homogeneous soils, the $B(z)$ curves in heterogeneous soils are larger because more biodegradation occurred in heterogeneous soils in most scenarios. Fig. 6 also shows that the variance in $B(z)$ across heterogeneous realizations is significantly larger for Monod biodegradation than first-order biodegradation, due to differences in reactant mixing patterns across each realization. For monocomponent biodegradation, the $B(z)$ curves of each individual heterogeneous realization are relatively smooth, and very similar to the heterogeneous average (Fig. 6a,b). For multicomponent biodegradation, the $B(z)$ curves of each individual heterogeneous realization fluctuate significantly with depth, but the heterogeneous average is relatively smooth (Fig. 6c,d). Therefore, although multicomponent biodegradation yields biomass distributions that are more spatially noisy within a small domain, a clear functional dependence with depth is obtained with bigger domains.

The horizontal coefficient of variation of biomass ($\eta_B = \sigma_B/\langle B\rangle$) quantifies how unevenly biomass is distributed across a horizontal layer of soil. Here, σ_B is the standard deviation of $B(z)$ in the horizontal direction calculated across all heterogeneous realizations. Such uneven distributions of biomass have previously been observed in groundwater aquifers (e.g. Vroblesky and Chapelle, 1994), in addition to hotspots of the associated biodegradation reaction products (Jobelius et al., 2011). For steady-state flow, Fig. 6e shows that η_B tends to increase with depth; more for first-order biodegradation than for multicomponent biodegradation. This is because first-order biodegradation occurs primarily in the preferential flow zones under steady-state flow. In contrast, Monod biodegradation mostly occurs in tandem with reactant mixing, and as a result is more spatially smoothed and less concentrated in preferential flow zones.

For transient flow scenarios (Fig. 6f), since the time of the flow rate transition is fixed across all 12 realizations, the maximum in η_B located in shallow soil corresponds to the plume's vertical position at the time of flow transition. This maximum in η_B occurs because the vertical location of the plume is different in the 12 heterogeneous realizations at the time of the transition. However, η_B decreases at depths traversed by the plume after the onset of transient flow, as the horizontal distribution of the reaction becomes spread more uniformly, due to preferential flow switching. Therefore, after a discrete transition from slow to fast infiltration rates, the vertical displacement of the contaminant plume becomes controlled by the cumulative infiltration and becomes less sensitive to heterogeneity, in agreement with French et al's (1999) findings for conservative solutes.

We also note that less mixing-limited scenarios (e.g. with mixing-independent first-order decay) have larger horizontal variances in biomass concentrations (solid lines in Fig. 6e and f), as contaminants biodegrade primarily within preferential flow zones. More mixing-limited scenarios have lower horizontal variances in biomass concentrations (dashed lines in Fig. 6e and f), because the reactions depend on dispersion and mixing to occur and are thus less confined to the main advection zones. Therefore, the extent of mixing-limitation of a scenario influences the spatial distribution of the microbial biomass growth, implying that the latter may be interpreted as a proxy indicator of mixing-limitation.

3.5. Implications for future research

A main result is that soil heterogeneity may decrease contaminant leaching to groundwater, due to enhanced reactant mixing, especially as biodegradation outcomes become increasingly limited by reactant mixing. In the laboratory or field, infiltration and leaching experiments can be performed on heterogeneous soils, with scenarios of varying extents of mixing-limitation. The extent of a scenario's mixing limitation can be controlled based on the mixing-limitation criteria that we have identified in Section 3.3. To further assess the mixing-limitation extent, the mixing-limitation criteria can be complemented with an additional analysis of the spatial distribution of microbial biomass, which we have elaborated on in the previous paragraph. Hence, our results may be reproduced in experimental or field settings by comparatively analyzing the leached fraction against the two indicators of mixing limitation that we have proposed: the mixing-limitation score, and the horizontal variance in microbial biomass distribution.

Further research may also be performed on the effects of other models of soil heterogeneity and preferential flow, such as mobile-immobile domain models, which explicitly distinguish between flow in soil matrices and macropores (Arora et al., 2011). In mobile-immobile domain models, the fraction of water in the immobile zone is typically defined by a constant parameter (e.g. Zhuang et al., 2021). Here, the mobile (preferential flow) and immobile (stagnant) zones do not

spatially shift as a result of transient flow, unlike under the random-field model of heterogeneity used in this study. However, other complexities arise under mobile-immobile domain models. For example, the volumetric capacities of the two domains, the solute diffusion rate between the two domains, and whether biodegradation occurs in both or only one of the two domains, would affect reactive solute fate in such models. Transient flow would complicate this further, as the sequences, frequencies, and amplitudes of transient infiltration events would interact with the mass transfer between the two domains. The segregation of the solute mass across the mobile and immobile domains would also interact strongly with the nonlinear Monod rate curve in determining contaminant biodegradation outcomes. We hypothesize that if biodegradation does not occur in one of the two domains (e.g. Brusseau et al., 1992), the presence of mobile-immobile domains will increase leaching, especially in more mixing-limited scenarios. This would be because segregating reactants into two compartments limits mixing, especially if the immobile domain accounts for a large fraction of pore space or the mass transfer rate is slow (Finkenbiner et al., 2022). If random-field soil hydraulic properties (as in this study) is coupled with mobile-immobile domains to represent soil heterogeneity, the problem remains highly complex, as demonstrated for conservative solutes (Talon et al., 2023). Other solute transport processes, such as nonequilibrium adsorption, may also affect biodegradation outcomes, through similarly complex interactions with random-field heterogeneity and transient flow (Radolinski et al., 2022).

Using Monod kinetics, we have modelled biodegradation as a multicomponent reaction with biomass growth, which accounts for how the biodegradation rate may increase over time. Another factor that could be researched in future studies is additional complexity in microbial biomass dynamics. For example, microbial biomass populations could decay to ambient levels if the microbes are unable to access or metabolize substrates for an extended amount of time (Nicol et al., 1994). For example, this may occur if the soil is deficient in organic hydrocarbons or electron acceptors (Geng et al., 2014). One could also consider the maximum possible biomass concentration, which would be reached when the microbial biomass (including live biomass and the organic matter associated with previously decayed biomass) occupies fully occupies the pore space available for biomass growth (Geng et al., 2015). Pore-space saturation with microbial biomass could interact significantly with soil heterogeneity. As the structures of heterogeneous soil matrices and pore spaces differ across space, so will the pore volumes available for biomass growth. Furthermore, as the pore spaces fill up with microbial biomass particles and their aggregates, the soil's permeability to water flow and the ability for electron acceptors to disperse through the pore spaces may decrease (Geng et al., 2016). This may also affect reactant mixing and overall biodegradation outcomes.

In the example of snowmelt infiltration described in this study, temperature fluctuations and freeze–thaw cycles (Zhang et al., 2023a) may also affect the dynamics of soil microbial biomass and the permeability of the soil matrix (Ni et al., 2018). This may ultimately alter contaminant transport and fate (Liu et al., 2022). In particular, freeze–thaw cycles may dynamically alter the heterogeneity of the soil matrix permeability: parts of pore space may become blocked or isolated by ice formation (Zhang et al., 2023b), while macroaggregates become fragmented (Leuther & Schlüter, 2021), leading to altered pore connectivities across the soil matrix (Rooney et al., 2022; Leuther & Schlüter, 2021). Existing evidence suggests that the hydraulic conductivity of the soil structure may increase gradually over time when the soil is subject to repeated freeze–thaw cycles (Leuther & Schlüter, 2021; Zhang et al., 2023b), even though the conductivity decreases temporarily while the soil is frozen. To account for the effects of temperature and freeze–thaw cycles, a possible approach is to use temperature-dependent biodegradation rates (El-Fadel et al., 1996), and soil porosities and permeabilities (Zhang et al., 2023a), coupled with an advection–dispersion model of heat transport (Tang & Rijnaarts, 2023).

In this study, the fact that t_{peak} can be used to perform a relative sensitivity analysis on the leached contaminant fraction through Da reinforces our earlier conclusion that the effect of transient flow on leaching outcomes is small. The information value of t_{peak} for biodegrading solutes is supported by existing literature on tracers and adsorbing (but non-biodegrading) solutes. Meyer-Windel et al. (1999) found that solute breakthrough in heterogeneous soils under transient flow can be more accurately predicted when the temporal coordinate is replaced by the cumulative drainage. Vanderborght et al (2000) showed that using the solute penetration depth is even more accurate than using the cumulative drainage. Hence, under transient flow, cumulative indicators of transport such as the cumulative drainage, solute penetration depth, and t_{peak} may be used to approximately assess solute fate. If such cumulative indicators are useful, then it implies that transient flow problems can be transformed to equivalent steady flow problems (Vanderborght et al., 2000). The predictive value of t_{peak} observed in this study suggests that such a coordinate transformation may also be possible for biodegrading contaminants. This could be an avenue for further research.

The implications of the modified Damköhler analysis finding also extends to the field. Suppose that the initial biodegradation rates $\frac{1}{C_0}\left(\frac{dC}{dt}\right)_{t=0}$ of various contaminants subject to various biogeochemical conditions are estimated through batch experiments in the laboratory, and parameterized as a first-order decay rate. On one hand, biodegradation rates observed in the field are widely known to be transient, and to differ greatly from biodegradation rates measured in the laboratory even under seemingly similar biogeochemical conditions (Greskowiak et al., 2017; Davis et al., 2003). Nevertheless, the relative persistence and mobility of the various contaminants observed in the laboratory translates well to the field, even when flow, transport, and biogeochemical conditions in the field are highly heterogeneous and transient (Narain-Ford et al., 2022). This is supported by our analysis of the information value of the modified Damköhler number Da, which depends only on the initial biodegradation rate (i.e., the biodegradation rate quantified in the laboratory) and mean contaminant residence time.

Another implication of our findings relate to the calibration of first-order contaminant decay rates from field data. The relative environmental fates of various contaminants predicted using simple one-dimensional homogeneous models with first-order decay, is popular in the literature and in policymaking (e.g. Rakonjac et al., 2023), due to their simplicity and broad applicability. As such first-order models predict a leached fraction of approximately $\exp(-\mu_{obs}t_{peak})$, observed first-order decay rates μ_{obs} inverted from field experiment data may be equivalent to $\frac{\beta}{C_0}\left(\frac{dC}{dt}\right)_{t=0}$ in the context of this study. If our numerical simulations correspond well to reality, then such simple and commonly-used first-order decay models may describe outcomes observed in reality well, even if first-order decay does not actually occur.

4. Conclusions

Multicomponent biodegradation of soil contaminants may be limited by the extent of mixing between reactants. As soil heterogeneity has been shown to increase mixing by a large body of literature, we hypothesized that contaminant biodegradation responds more positively to soil heterogeneity if the reaction is more mixing-limited. We identify three conditions that imply that biodegradation in a scenario is limited by mixing. When these conditions are fulfilled, mixing contributes on average towards increasing the biodegradation rate (Section 3.3). This proposition is validated with numerical simulations. We show that in cases where contaminant biodegradation is mixing-limited, the presence of soil heterogeneity more likely reduces the fraction of contaminants that leach through the unsaturated zone.

Accordingly, the widespread general notion that soil heterogeneity must increase contaminant leaching is generally accurate only in the limiting situation that biodegradation rates are independent of reactant mixing. A previous study showed that heterogeneity may facilitate

biodegradation under steady-state flow in the saturated zone (Bauer et al., 2009). In this study, we extend this notion to the unsaturated zone and transient flow for the first time, in particular for mixing-limited reactions. Future research could focus on whether this conclusion also applies to soil columns with different thicknesses. We have shown that multicomponent biodegradation mostly occurs at some depth in the subsurface, as reactants require time and space to mix. Conversely, first-order decay mostly occurs at the topsoil. This suggests that the additional mixing contributed by soil heterogeneity may make a smaller difference to overall contaminant biodegradation outcomes in thicker soil columns, where ample mixing can occur even if the soil was homogeneous.

We were unable to identify and isolate any consistent effects, of the interactions between soil heterogeneity and transient flow, on contaminant fate. Hence, transient flow does not seem to make a difference to the observation that soil heterogeneity tends to decrease leaching in mixing-limited scenarios. In heterogeneous soils, although transient flow causes dynamic preferential flow zone switching, increasing the interfacial area for mixing between plumes, it may also cause contaminant fluxes to bypass established microbial biomass hotspots. The latter is evident in that the horizontal spatial variability of biomass in heterogeneous soils is less heterogeneous under transient flow, than under steady-state flow. Hence, the influence of transient flow on contaminant fate is likely to be highly scenario-dependent, and thus not as generalizable as the effects of soil heterogeneity. Therefore, if both soil heterogeneity and transient flow are present, it is important to simulate both simultaneously, especially for mixing-limited scenarios. This is because interaction effects between soil heterogeneity and transient flow may greatly affect mixing, and would not be accounted for otherwise. Nevertheless, the information value we have found for simple observables, such as the peak breakthrough time t_{peak} and the initial biodegradation rate $\frac{1}{C_0}\left(\frac{dC}{dt}\right)_{t=0}$, suggest that the piling up of multiple nonlinear complexities (soil heterogeneity, transient flow, multicomponent kinetics, biomass growth) may bring about some degree of emergent simplicity in overall contaminant fate. It would be interesting to study how the addition of more processes to the model, such as temperature-dependent biodegradation rates, freeze–thaw cycles, and mobile-immobile domains, would affect the viability of inferring such coarse but general outcomes of contaminant fate under complex conditions. Emergent simplicity under highly complex conditions should be pursued in future research on this topic, as it has already yielded significant insight in other fields of hydrology (McColl & Rigden, 2020) and science in general (Wang, 2018).

CRediT authorship contribution statement

Darrell W.S. Tang: Conceptualization, Formal analysis, Investigation, Methodology, Writing – original draft. **Helen K. French:** Writing – review & editing, Conceptualization. **Anton Leijnse:** Supervision, Conceptualization. **Ruud P. Bartholomeus:** Writing – review & editing, Supervision. **Sjoerd E.A.T.M. van der Zee:** Writing – review & editing, Supervision, Conceptualization.

Declaration of competing interest

The authors declare that they have no known competing financial interests or personal relationships that could have appeared to influence the work reported in this paper.

Data availability

No data was used for the research described in the article.

Acknowledgements

This research was conducted in the context of the project “Re-Use of Treated effluent for agriculture RUST” of the Closed Cycles program and was funded by the Netherlands Organization for Scientific Research under contract NWOGK.2016.016. This work was initiated and partly supported by the Research Council of Norway (FRINATEK project 213407, In-situ redox).

Appendix A. Supplementary data

Supplementary data to this article can be found online at https://doi.org/10.1016/j.jhydrol.2024.131111.

References

Acharya, R.C., Van der Zee, S.E.A.T.M., Leijnse, A., 2005. Transport modelling of nonlinearly adsorbing solutes in physically heterogeneous pore networks. Water Resour. Res. 41 (2).
Arora, B., Mohanty, B.P., McGuire, J.T., 2011. Inverse estimation of parameters for multidomain flow models in soil columns with different macropore densities. Water Resour. Res. 47 (4).
Barrios, R.E., Gaonkar, O., Snow, D., Li, Y., Li, X., Bartelt-Hunt, S.L., 2019. Enhanced biodegradation of atrazine at high infiltration rates in agricultural soils. Environ. Sci. Processes Impacts 21 (6), 999–1010.
Barry, D.A., Prommer, H., Miller, C.T., Engesgaard, P., Brun, A., Zheng, C., 2002. Modelling the fate of oxidisable organic contaminants in groundwater. Adv. Water Resour. 25 (8–12), 945–983.
Batalha, M.S., Barbosa, M.C., Faybishenko, B., Van Genuchten, M.T., 2018. Effect of temporal averaging of meteorological data on predictions of groundwater recharge. J. Hydrol. Hydromech. 66 (2), 143–152.
Battiato, I., Tartakovsky, D.M., Tartakovsky, A.M., Scheibe, T., 2009. On breakdown of macroscopic models of mixing-controlled heterogeneous reactions in porous media. Adv. Water Resour. 32 (11), 1664–1673.
Bauer, R.D., Maloszewski, P., Zhang, Y., Meckenstock, R.U., Griebler, C., 2008. Mixing-controlled biodegradation in a toluene plume—results from two-dimensional laboratory experiments. J. Contam. Hydrol. 96 (1–4), 150–168.
Bauer, R.D., Rolle, M., Bauer, S., Eberhardt, C., Grathwohl, P., Kolditz, O., Griebler, C., 2009. Enhanced biodegradation by hydraulic heterogeneities in petroleum hydrocarbon plumes. J. Contam. Hydrol. 105 (1–2), 56–68.
Beltman, W.H.J., Boesten, J.J.T.I., Van der Zee, S.E.A.T.M., 1995. Analytical modelling of pesticide transport from the soil surface to a drinking water well. J. Hydrol. 169 (1–4), 209–228.
Benson, D.A., Aquino, T., Bolster, D., Engdahl, N., Henri, C.V., Fernandez-Garcia, D., 2017. A comparison of Eulerian and Lagrangian transport and non-linear reaction algorithms. Adv. Water Resour. 99, 15–37.
Birkholzer, J., Tsang, C.F., 1997. Solute channeling in unsaturated heterogeneous porous media. Water Resour. Res. 33 (10), 2221–2238.
Biró, B., Toscano, G., Horváth, N., Matics, H., Domonkos, M., Scotti, R., Rao, M.A., Wejden, B., French, H.K., 2014. Vertical and horizontal distributions of microbial abundances and enzymatic activities in propylene-glycol-affected soils. Environ. Sci. Pollut. Res. 21 (15), 9095–9108.
Blum, P., Hunkeler, D., Weede, M., Beyer, C., Grathwohl, P., Morasch, B., 2009. Quantification of biodegradation for o-xylene and naphthalene using first order decay models, Michaelis-Menten kinetics and stable carbon isotopes. J. Contam. Hydrol. 105 (3–4), 118–130.
Brusseau, M.L., Jessup, R.E., Rao, P.S.C., 1992. Modeling solute transport influenced by multiprocess nonequilibrium and transformation reactions. Water Resour. Res. 28 (1), 175–182.
Carsel, R.F., Parrish, R.S., 1988. Developing joint probability distributions of soil water retention characteristics. Water Resour. Res. 24 (5), 755–769.
Cirpka, O.A., de Barros, F.P., Chiogna, G., Rolle, M., Nowak, W., 2011. Stochastic flux-related analysis of transverse mixing in two-dimensional heterogeneous porous media. Water Resour. Res. 47 (6).
Cirpka, O.A., Valocchi, A.J., 2007. Two-dimensional concentration distribution for mixing-controlled bioreactive transport in steady state. Adv. Water Resour. 30 (6–7), 1668–1679. https://doi.org/10.1016/j.advwatres.2006.05.022.
Corwin, D.L., Rhoades, J.D., Šimůnek, J., 2007. Leaching requirement for soil salinity control: Steady-state versus transient models. Agric. Water Manag. 90 (3), 165–180.
Davis, C., Cort, T., Dai, D., Illangasekare, T.H., Munakata-Marr, J., 2003. Effects of heterogeneity and experimental scale on the biodegradation of diesel. Biodegradation 14, 373–384.
De Vries, J. (2016). Solute transport and water flow in an unsaturated, heterogeneous profile with root water uptake (MSc thesis, Wageningen University).
De Wilde, T., Mertens, J., Šimunek, J., Sniegowksi, K., Ryckeboer, J., Jaeken, P., Spanoghe, P., 2009. Characterizing pesticide sorption and degradation in microscale biopurification systems using column displacement experiments. Environ. Pollut. 157 (2), 463–473.
El-Fadel, M., Findikakis, A.N., Leckie, J.O., 1996. Temperature effects in modeling solid waste biodegradation. Environ. Technol. 17 (9), 915–935.

Finkenbiner, C.E., Good, S.P., Renée Brooks, J., Allen, S.T., Sasidharan, S., 2022. The extent to which soil hydraulics can explain ecohydrological separation. Nat. Commun. 13 (1), 6492.
French, H., Binley, A., 2004. Snowmelt infiltration: monitoring temporal and spatial variability using time-lapse electrical resistivity. J. Hydrol. 297 (1–4), 174–186.
French, H.K., Van der Zee, S.E.A.T.M., Leijnse, A., 1999. Differences in gravity-dominated unsaturated flow during autumn rains and snowmelt. Hydrol. Process. 13 (17), 2783–2800.
French, H.K., Van der Zee, S.E.A.T.M., Leijnse, A., 2001. Transport and degradation of propyleneglycol and potassium acetate in the unsaturated zone. J. Contam. Hydrol. 49 (1–2), 23–48.
French, H.K., Hansen, M.C., Moe, K.G., Stene, J., 2023. Modelling plume development with annual pulses of contaminants released from an airport runway to a layered aquifer, evaluation of an in situ monitoring system. Water 15 (5), 985.
Geng, X., Boufadel, M.C., Personna, Y.R., Lee, K., Tsao, D., Demicco, E.D., 2014. BioB: a mathematical model for the biodegradation of low solubility hydrocarbons. Mar. Pollut. Bull. 83 (1), 138–147.
Geng, X., Boufadel, M.C., Lee, K., Abrams, S., Suidan, M., 2015. Biodegradation of subsurface oil in a tidally influenced sand beach: Impact of hydraulics and interaction with pore water chemistry. Water Resour. Res. 51 (5), 3193–3218.
Geng, X., Pan, Z., Boufadel, M.C., Ozgokmen, T., Lee, K., Zhao, L., 2016. Simulation of oil bioremediation in a tidally influenced beach: Spatiotemporal evolution of nutrient and dissolved oxygen. J. Geophys. Res. Oceans 121 (4), 2385–2404.
Gouet-Kaplan, M., Arye, G., Berkowitz, B., 2012. Interplay between resident and infiltrating water: Estimates from transient water flow and solute transport. J. Hydrol. 458, 40–50.
Gray, D.M., Toth, B., Zhao, L., Pomeroy, J.W., Granger, R.J., 2001. Estimating areal snowmelt infiltration into frozen soils. Hydrol. Process. 15 (16), 3095–3111.
Greskowiak, J., Hamann, E., Burke, V., Massmann, G., 2017. The uncertainty of biodegradation rate constants of emerging organic compounds in soil and groundwater–A compilation of literature values for 82 substances. Water Res. 126, 122–133.
Grösbacher, M., Eckert, D., Cirpka, O.A., Griebler, C., 2018. Contaminant concentration versus flow velocity: Drivers of biodegradation and microbial growth in groundwater model systems. Biodegradation 29 (3), 211–232.
Hesse, F., Radu, F.A., Thullner, M., Attinger, S., 2009. Upscaling of the advection–diffusion–reaction equation with Monod reaction. Adv. Water Resour. 32 (8), 1336–1351.
Hickman, G.T., Novak, J.T., 1989. Relationship between subsurface biodegradation rates and microbial density. Environ. Sci. Tech. 23 (5), 525–532.
Holden, P.A., Fierer, N., 2005. Microbial processes in the vadose zone. Vadose Zone J. 4 (1), 1–21.
Hubert, A., Aquino, T., Tabuteau, H., Méheust, Y., Le Borgne, T., 2020. Enhanced and non-monotonic effective kinetics of solute pulses under Michaelis-Menten reactions. Adv. Water Resour. 146, 103739.
Hunter, K.S., Wang, Y., Van Cappellen, P., 1998. Kinetic modeling of microbially-driven redox chemistry of subsurface environments: coupling transport, microbial metabolism and geochemistry. J. Hydrol. 209 (1–4), 53–80.
Jobelius, C., Ruth, B., Griebler, C., Meckenstock, R.U., Hollender, J., Reineke, A., Zwiener, C., 2011. Metabolites indicate hot spots of biodegradation and biogeochemical gradients in a high-resolution monitoring well. Environ. Sci. Tech. 45 (2), 474–481.
Jury, W.A., Gruber, J., 1989. A stochastic analysis of the influence of soil and climatic variability on the estimate of pesticide groundwater pollution potential. Water Resour. Res. 25 (12), 2465–2474.
Kass, A., Gavrieli, I., Yechieli, Y., Vengosh, A., Starinsky, A., 2005. The impact of freshwater and wastewater irrigation on the chemistry of shallow groundwater: A case study from the Israeli Coastal Aquifer. J. Hydrol. 300 (1–4), 314–331.
Kirillin, G., Leppäranta, M., Terzhevik, A., Granin, N., Bernhardt, J., Engelhardt, C., Zdorovennov, R., 2012. Physics of seasonally ice-covered lakes: A review. Aquat. Sci. 74, 659–682.
Kuntz, D., Grathwohl, P., 2009. Comparison of steady-state and transient flow conditions on reactive transport of contaminants in the vadose soil zone. J. Hydrol. 369 (3–4), 225–233.
Leuther, F., Schlüter, S., 2021. Impact of freeze–thaw cycles on soil structure and soil hydraulic properties. Soil 7 (1), 179–191.
Li, L., Peters, C.A., Celia, M.A., 2006. Upscaling geochemical reaction rates using pore-scale network modelling. Adv. Water Resour. 29 (9), 1351–1370.
Liu, H., Hu, Y., Hao, Y., Yan, X., Wu, L., Wang, C., Li, X., 2022. Progressive freeze-thaw redistributes water, solute and CO_2 emissions across soil layers–The role of soil particle size. Catena 219, 106614.
Luo, J., Dentz, M., Carrera, J., Kitanidis, P., 2008. Effective reaction parameters for mixing controlled reactions in heterogeneous media. Water Resour. Res. 44 (2).
Mayer, K.U., Frind, E.O., Blowes, D.W., 2002. Multicomponent reactive transport modeling in variably saturated porous media using a generalized formulation for kinetically controlled reactions. Water Resour. Res. 38 (9), 13.
McColl, K.A., Rigden, A.J., 2020. Emergent simplicity of continental evapotranspiration. Geophys. Res. Lett. 47 (6).
Meyer-Windel, S., Lennartz, B., Widmoser, P., 1999. Bromide and herbicide transport under steady-state and transient flow conditions. Eur. J. Soil Sci. 50 (1), 23–33.
Miller, E.E., Miller, R.D., 1956. Physical theory for capillary flow phenomena. J. Appl. Phys. 27 (4), 324–332.
Mohamed, M.M., Hatfield, K., Hassan, A.E., 2006. Monte Carlo evaluation of microbial-mediated contaminant reactions in heterogeneous aquifers. Adv. Water Resour. 29 (8), 1123–1139.
Moreno, L., Tsang, C.F., 1994. Flow channeling in strongly heterogeneous porous media: A numerical study. Water Resour. Res. 30 (5), 1421–1430.
Mulligan, C.N., Yong, R.N., 2004. Natural attenuation of contaminated soils. Environ. Int. 30 (4), 587–601.
Narain-Ford, D.M., van Wezel, A.P., Helmus, R., Dekker, S.C., Bartholomeus, R.P., 2022. Soil self-cleaning capacity: Removal of organic compounds during sub-surface irrigation with sewage effluent. Water Res. 226, 119303.
Ni, Z., van Gaans, P., Rijnaarts, H., Grotenhuis, T., 2018. Combination of aquifer thermal energy storage and enhanced bioremediation: Biological and chemical clogging. Sci. Total Environ. 613, 707–713.
Nicol, J.P., Wise, W.R., Molz, F.J., Benefield, L.D., 1994. Modeling biodegradation of residual petroleum in a saturated porous column. Water Resour. Res. 30 (12), 3313–3325.
Olsen, L., Sveian, H., Ottesen, D., & Rise, L. (2013). Quaternary glacial, interglacial and interstadial deposits of Norway and adjacent onshore and offshore areas. Quaternary Geology of Norway, Geological Survey of Norway Special Publication, 13, 79-144.
Parkhurst, D., Appelo, C.A.J., 2013. PHREEQC (version 3)—A computer program for speciation, batch-reaction, one-dimensional transport, and inverse geochemical calculations. Water Resour. Invest. Rep. 99–4259.
Pedretti, D., Fernàndez-Garcia, D., Bolster, D., Sanchez-Vila, X., 2013. On the formation of breakthrough curves tailing during convergent flow tracer tests in three-dimensional heterogeneous aquifers. Water Resour. Res. 49 (7), 4157–4173.
Pressl, A., Pucher, B., Scharf, B., Langergraber, G., 2019. Treatment of de-icing contaminated surface water runoff along an airport runway using in-situ soil enriched with structural filter materials. Sci. Total Environ. 660, 321–328.
Puyguiraud, A., Perez, L.J., Hidalgo, J.J., Dentz, M., 2020. Effective dispersion coefficients for the upscaling of pore-scale mixing and reaction. Adv. Water Resour. 146, 103782.
Radolinski, J., Le, H., Hilaire, S.S., Xia, K., Scott, D., Stewart, R.D., 2022. A spectrum of preferential flow alters solute mobility in soils. Sci. Rep. 12 (1), 4261.
Rakonjac, N., van der Zee, S.E., Wipfler, L., Roex, E., Urbina, C.F., Borgers, L.H., Ritsema, C.J., 2023. An analytical framework on the leaching potential of veterinary pharmaceuticals: A case study for the Netherlands. Sci. Total Environ. 859, 160310.
Ramalingam, V., Cupples, A.M., 2020. Anaerobic 1, 4-dioxane biodegradation and microbial community analysis in microcosms inoculated with soils or sediments and different electron acceptors. Appl. Microbiol. Biotechnol. 104, 4155–4170.
Rodziewicz, J., Mielcarek, A., Janczukowicz, W., Ostrowska, K., Jóźwiakowski, K., Bugajski, P., Jucherski, A., 2020. Biofilter with innovative filling for low-temperature treatment of sewage from de-icing airport runways. Sep. Purif. Technol. 242, 116761.
Rolle, M., Eberhardt, C., Chiogna, G., Cirpka, O.A., Grathwohl, P., 2009. Enhancement of dilution and transverse reactive mixing in porous media: Experiments and model-based interpretation. J. Contam. Hydrol. 110 (3–4), 130–142.
Rolle, M., Le Borgne, T., 2019. Mixing and reactive fronts in the subsurface. Rev. Mineral. Geochem. 85 (1), 111–142.
Rooney, E.C., Bailey, V.L., Patel, K.F., Dragila, M., Battu, A.K., Buchko, A.C., Lybrand, R. A., 2022. Soil pore network response to freeze-thaw cycles in permafrost aggregates. Geoderma 411, 115674.
Roth, K., 1995. Steady state flow in an unsaturated, two-dimensional, macroscopically homogeneous, miller-similar medium. Water Resour. Res. 31 (9), 2127–2140.
Sander, G.C., Braddock, R.D., 2005. Analytical solutions to the transient, unsaturated transport of water and contaminants through horizontal porous media. Adv. Water Resour. 28 (10), 1102–1111.
Schotanus, D., van der Ploeg, M.J., van der Zee, S.E.A.T.M., 2012. Quantifying heterogeneous transport of a tracer and a degradable contaminant in the field, with snowmelt and irrigation. Hydrol. Earth Syst. Sci. 16 (8).
Schotanus, D., van der Ploeg, M.J., Zee, S.E.A.T.M., 2013. Spatial distribution of solute leaching with snowmelt and irrigation: measurements and simulations. Hydrol. Earth Syst. Sci. 17 (4), 1547–1560.
Schotanus, D., Meeussen, J.C.L., Lissner, H., van der Ploeg, M.J., Wehrer, M., Totsche, K. U., van der Zee, S.E.A.T.M., 2014. Transport and degradation of propylene glycol in the vadose zone: model development and sensitivity analysis. Environ. Sci. Pollut. Res. 21 (15), 9054–9066.
Shen, J., Chen, Y., Wu, S., Wu, H., Liu, X., Sun, X., Wang, L., 2015. Enhanced pyridine biodegradation under anoxic condition: The key role of nitrate as the electron acceptor. Chem. Eng. J. 277, 140–149.
Šimůnek, J., Jacques, D., Šejna, M., & van Genuchten, M.T. (2012a). The HP2 program for HYDRUS (2D/3D): A coupled code for simulating two-dimensional variably-saturated water flow, heat transport, and biogeochemistry in porous media, version 1.0. PC Progress, Prague, Czech Republic.
Šimůnek, J., Van Genuchten, M.T., & Šejna, M. (2012b). The HYDRUS software package for simulating two-and three-dimensional movement of water, heat, and multiple solutes in variably-saturated media. Technical manual, version 2.
Šimůnek, J., Šejna, M., Saito, H., Sakai, M., Th. van Genuchten, M. (2013) The Hydrus-1D Software Package for Simulating the Movement of Water, Heat, and Multiple Solutes in Variably Saturated Media, Version 4.17, HYDRUS Software Series 3, Department of Environmental Sciences, University of California Riverside, Riverside, California, USA, pp. 342.
Singh, D.K., 2008. Biodegradation and bioremediation of pesticide in soil: concept, method and recent developments. Indian J. Microbiol. 48 (1), 35–40.
Song, X., Seagren, E.A., 2008. In situ bioremediation in heterogeneous porous media: Dispersion-limited scenario. Environ. Sci. Tech. 42 (16), 6131–6140.
Soulas, G., Lagacherie, B., 2001. Modelling of microbial degradation of pesticides in soils. Biol. Fertil. Soils 33 (6), 551–557.
Talon, L., Ollivier-Triquet, E., Dentz, M., Bauer, D., 2023. Transient dispersion regimes in heterogeneous porous media: On the impact of spatial heterogeneity in permeability

and exchange kinetics in mobile–immobile transport. Adv. Water Resour. 174, 104425.
Tang, D., Rijnaarts, H.H.M., 2023. Dimensionless thermal efficiency analysis for aquifer thermal energy storage. Water Resour. Res. 59 (11).
Tang, D.W.S., van der Zee, S.E.A.T.M., Narain-Ford, D.M., van den Eertwegh, G.A.P.H., Bartholomeus, R.P., 2023. Managed phreatic zone recharge for irrigation and wastewater treatment. J. Hydrol. 626, 130208.
Ursino, N., Gimmi, T., Flühler, H., 2001. Dilution of non-reactive tracers in variably saturated sandy structures. Adv. Water Resour. 24 (8), 877–885.
Valocchi, A.J., Bolster, D., Werth, C.J., 2019. Mixing-limited reactions in porous media. Transp. Porous Media 130 (1), 157–182.
van der Zee, S.E.A.T.M., Boesten, J.J., 1991. Effects of soil heterogeneity on pesticide leaching to groundwater. Water Resour. Res. 27 (12), 3051–3063.
Vanderborght, J., Jacques, D., Feyen, J., 2000. Deriving transport parameters from transient flow leaching experiments by approximate steady-state flow convection–dispersion models. Soil Sci. Soc. Am. J. 64 (4), 1317–1327.
Vereecken, H., Kasteel, R., Vanderborght, J., Harter, T., 2007. Upscaling hydraulic properties and soil water flow processes in heterogeneous soils: A review. Vadose Zone J. 6 (1), 1–28.
Voigt, C., Marushchak, M.E., Abbott, B.W., Biasi, C., Elberling, B., Siciliano, S.D., Martikainen, P.J., 2020. Nitrous oxide emissions from permafrost-affected soils. Nat. Rev. Earth Environ. 1 (8), 420–434.
Vroblesky, D.A., Chapelle, F.H., 1994. Temporal and spatial changes of terminal electron-accepting processes in a petroleum hydrocarbon-contaminated aquifer and the significance for contaminant biodegradation. Water Resour. Res. 30 (5), 1561–1570.
Wang, S., 2018. Simplicity from complex interactions. Nat. Ecol. Evol. 2 (8), 1201–1202.
Warrick, A.W., Biggar, J.W., Nielsen, D.R., 1971. Simultaneous solute and water transfer for an unsaturated soil. Water Resour. Res. 7 (5), 1216–1225.
Werth, C.J., Cirpka, O.A., Grathwohl, P., 2006. Enhanced mixing and reaction through flow focusing in heterogeneous porous media. Water Resour. Res. 42 (12).
Widdel, F., Musat, F., Knittel, K., Galushko, A., 2007. Anaerobic Degradation of Hydrocarbons With Sulphate as Electron Acceptor. Sulphate-Reducing Bacteria. Cambridge University Press, Cambridge.
Willingham, T., Zhang, C., Werth, C.J., Valocchi, A.J., Oostrom, M., Wietsma, T.W., 2010. Using dispersivity values to quantify the effects of pore-scale flow focusing on enhanced reaction along a transverse mixing zone. Adv. Water Resour. 33 (4), 525–535.
Yu, X., Michael, H.A., 2022. Impacts of the scale of representation of heterogeneity on simulated salinity and saltwater circulation in coastal aquifers. Water Resour. Res. 58 (1).
Yuan, F., Meixner, T., Fenn, M.E., Šimůnek, J., 2011. Impact of transient soil water simulation to estimated nitrogen leaching and emission at high-and low-deposition forest sites in Southern California. J. Geophys. Res. Biogeo. 116 (G3).
Zhang, J., Lai, Y., Li, S., Zhang, M., You, Z., Liang, T., 2023a. Numerical study on the spatial–temporal distribution of solute and salt accumulation in saturated sulfate saline soil during freezing–thawing processes: Mechanism and feedback. Adv. Water Resour. 177, 104461.
Zhang, Z., Wang, Y., Ma, Z., Lv, M., 2023b. Response mechanism of soil structural heterogeneity in permafrost active layer to freeze–thaw action and vegetation degradation. Catena 230, 107250.
Zhuang, L., Raoof, A., Mahmoodlu, M.G., Biekart, S., de Witte, R., Badi, L., Lin, K., 2021. Unsaturated flow effects on solute transport in porous media. J. Hydrol. 598, 126301.